An Improved Generalized Average Model of DC–DC Dual Active Bridge Converters

Jacob A. Mueller, *Student Member, IEEE* and Jonathan W. Kimball, *Senior Member, IEEE*

***Abstract*—Improvements are proposed for generalized average models of dual active bridge (DAB) converters. Generalized average modeling involves a tradeoff between accuracy and tractability. To maintain an acceptable level of complexity, existing DAB models are derived using a first harmonic approximation. These models provide accurate small-signal representations, but are limited as large-signal analysis tools due to persistent steady-state error. This study proposes a modeling framework that provides accurate large and small-signal models without significant increases in the overall complexity. The framework describes DAB operation with a triple phase shift modulation, and is easily simplified for single, dual, or extended phase shift modulation schemes. The special case of a single phase shift modulation, which experiences the most significant large-signal error, is given additional consideration. The framework is applied to open and closed-loop operation, and both large- and small-signal models are discussed. Models are validated in simulation and hardware experiments using a small scale DAB prototype.**

***Index Terms*—Average modeling, dual active bridge (DAB) converter, generalized average model, phase shift modulation.**

I. Introduction

THE dual active bridge (DAB) topology features desirable performance characteristics including galvanic isolation, high power density, low device stresses, and bidirectional operation [1], [2]. Many of these attributes are due to a high-frequency ac conversion stage. However, the associated ac state variables present challenges when developing models of the converter's behavior. In particular, the transformer current state precludes the "small-ripple" approximation commonly employed in traditional modeling approaches, e.g., state-space averaging and average circuit modeling.

Previous studies have addressed the challenges of modeling DAB converters. The most common strategy uses the sampled-data modeling procedure from [3] to develop discrete-time models. This approach was used in [4] to develop an open-loop DAB model, and again in [5] to develop a more detailed model consisting of a converter, EMI filters, and control system. In these models, the converter transitions through discrete modes of operation, each described by a set of linear time-invariant ordinary differential equations (ODEs). The transition times are either explicitly controlled (e.g., by gate driver signals) or implicitly determined by device thresholds (e.g., by diode current zero crossings). The state solution within each mode is explicitly determined by initial conditions at transition times and state transition matrices consisting of matrix exponentials. In [6], matrix exponential calculations were avoided through the use of bilinear approximations, leading to a simplified discrete-time DAB model.

The advantage of the discrete-time models in [4]–[6] is that they explicitly describe state trajectories in all subintervals of converter operation, meaning that they are capable of providing exact solutions for ac state variables. In the case of DAB converters, these models are able to accurately predict transformer currents and, as in [4], the current zero crossings critical to zero voltage switching (ZVS) [7]. The capabilities of discrete-time representations notwithstanding, two factors motivate the development of accurate continuous-time models. First, continuous-time models are still preferred for control design due to the prevalence of simple and powerful design tools. Second, DAB converters are well-suited to applications in multiconverter systems, such as solid-state transformers [8], microgrids, and dc distribution systems. The framework of [3] assumes cyclic transitions through fully characterized modes of operation, and is not intended to produce models that are modular elements of a larger system. Representing all possible switching modes at the system level quickly becomes infeasible as the number of converters increases. Moreover, differences in converter switching frequencies make it difficult to define a usable system-wide base period. For the purposes of a system-level analysis, more scalable alternatives are required.

Continuous-time DAB models have been proposed as well. The simplest model, proposed in [9], essentially results from the application of classical state-space averaging [10]. Since the dc average of transformer current is 0, the state is eliminated in the averaging process, and its dynamics are lost in the final model. A more detailed approach was used in [11] to derive both large and small-signal average models. The ac stage in these models is represented by half period averages of the dc currents into and out of the H-bridges. This allows the models to incorporate effects of transformer core and conduction losses, which are omitted from the models in [9]. A similar procedure was used in [12] for the purposes of a steady-state analysis.

A continuous-time DAB model was derived using generalized average modeling (GAM) in [13]. In GAM, state variables are

Manuscript received December 8, 2017; accepted January 15, 2018. Date of publication January 25, 2018; date of current version August 7, 2018. Recommended for publication by Associate Editor Dr. Santanu Kapat. *(Corresponding author: Jacob A. Mueller.)*

The authors are with the Department of Electrical and Computer Engineering, Missouri University of Science and Technology, Rolla MO 65409 USA (e-mail: jam8z4@mst.edu; kimballjw@mst.edu).

Color versions of one or more of the figures in this paper are available online at http://ieeexplore.ieee.org.

Digital Object Identifier 10.1109/TPEL.2018.2797966

See http://www.ieee.org/publications_standards/publications/rights/index.html for more information.

expanded into Fourier series terms at multiples of the converter switching frequency [14], providing straightforward representations of ac states. However, the GAM framework involves a tradeoff between the accuracy and complexity. Specifically, both the accuracy and complexity increase with the number of Fourier series terms included in the model. The model in [13] uses a first harmonic approximation, and truncates the Fourier series at the first harmonic. When linearized, the model accurately predicts small-signal responses, but the large-signal model is inaccurate at the steady state. The accuracy of the model increases when more Fourier series terms are included (see, e.g., [15]), but the number of model states increases rapidly with the number of Fourier series terms considered, so even small accuracy gains require substantial penalties in terms of model complexity.

This steady-state error was previously noted in [11], and a method of correcting the error was proposed in [16]. The approach in [16] consists of applying a multiplicative correction factor to the load and state variables. However, the correction factor is only derived for a single phase shift operation. Furthermore, the method assumes lossless operation, and neglects the effect of transformer winding resistance, which may be significant in practice. This copper loss is particularly important for a single phase shift operation, which produces large circulating currents, or when the ratio of winding resistance to leakage reactance is high [12].

This study presents the following contributions:

1) The DAB model from [13] is extended to more general modulation strategies, including dual, extended, and triple phase shift modulation. Both large- and small-signal models are described.
2) A new method of eliminating the error caused by truncating the Fourier series at the first harmonic is proposed. The method involves deriving the relationship between the equilibrium solution to the model equations and exact steady-state expressions, and then including those relationships in the model itself.
3) An additional correction factor that includes copper losses in the transformer is derived for the special case of single phase shift modulation.

The structure of the paper is as follows. Section II briefly reviews the DAB model from [13] and describes the steady-state model error in precise terms. The improved DAB model is given in Section III, starting with the extension to more general modulation strategies, and then including the large-signal error correction. Model partial derivatives, including those necessary to develop small-signal models, are given in Section IV. Special consideration is given to the single phase shift case in Section V, including the derivation of a lossy correction factor. Verification experiments are described in Section VI.

II. Background

This section reviews the DAB model from [13] to be improved in the following section, establishes important terms and notation, and provides a mathematical description of the steady-state error problem.

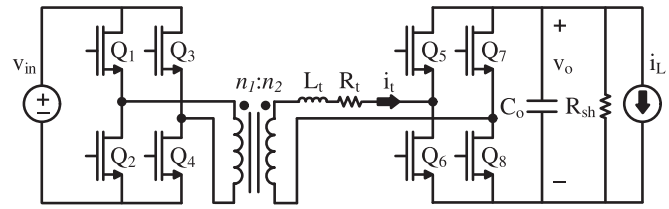

Fig. 1. DAB topology.

A. Original DAB Model

The original DAB model proposed in [13] begins with

$$\dot{v}_o = \frac{-1}{R_{sh}C_o}v_o + \frac{1}{C_o}i_t s_2(\tau, d) - \frac{1}{C_o}i_L \tag{1}$$

$$\dot{i}_t = \frac{1}{L_t}v_{\text{in}}s_1(\tau, d) - \frac{1}{L_t}v_o s_2(\tau, d) - \frac{R_t}{L_t}i_t \tag{2}$$

where dot notations are used to indicate derivatives with respect to time. The signals and parameters in these equations are identified in Fig. 1. All hardware parameters are referred to the secondary side of the transformer. For simplicity, the derivation shown here assumes a 1:1 turns ratio. The only modification necessary to include nonunity turns ratios in the model is to replace all appearances of v_{in} with $\frac{n_2}{n_1}v_{\text{in}}$. This is true for this model and for the models proposed in the following section.

$s_1(\tau, d)$ and $s_2(\tau, d)$ are the switching signals that drive the input and output H-bridges, respectively. The model from [13] was derived for a single phase shift modulation. For time τ in a switching interval ($0 \le \tau < T$) and phase shift argument d, the single phase shift switching signals are as follows:

$$s_1(\tau, d) = \begin{cases} 1, & 0 \le \tau < \frac{T}{2} \\ -1, & \frac{T}{2} \le \tau < T \end{cases} \tag{3}$$

$$s_2(\tau, d) = \begin{cases} 1, & \frac{dT}{2} \le \tau < \frac{dT}{2} + \frac{T}{2} \\ -1, & 0 \le \tau < \frac{dT}{2} \text{ or } \frac{dT}{2} + \frac{T}{2} \le \tau < T \end{cases}. \tag{4}$$

At this point, the GAM framework and first harmonic approximation are applied. The following equations include a critical change: the phase shift variable, represented as d in the switching signal definitions, becomes a new variable $\hat{d}$. The reasons for this are discussed in the following section, but the change first appears here because it is a direct consequence of the first harmonic approximation. The GAM state equations are as follows:

$$\dot{\langle v_o \rangle}_0 = \frac{-1}{R_{sh}C_o}\langle v_o \rangle_0 - \frac{4\sin\pi\hat{d}}{C_o\pi}\langle i_t \rangle_R - \frac{4\cos\pi\hat{d}}{C_o\pi}\langle i_t \rangle_I - \frac{\langle i_L \rangle_0}{C_o} \tag{5}$$

$$\dot{\langle i_t \rangle}_R = \frac{2\sin\pi\hat{d}}{L_t\pi}\langle v_o \rangle_0 - \frac{R_t}{L_t}\langle i_t \rangle_R + \omega_s\langle i_t \rangle_I \tag{6}$$

$$\dot{\langle i_t \rangle}_I = \frac{2\cos\pi\hat{d}}{L_t\pi}\langle v_o \rangle_0 - \omega_s\langle i_t \rangle_R - \frac{R_t}{L_t}\langle i_t \rangle_I - \frac{2\langle v_{\text{in}} \rangle_0}{L_t\pi}. \tag{7}$$

The states of the model are the dc average output capacitor voltage and the real/imaginary components of the fundamental

harmonic transformer current. The model inputs are the source voltage, phase shift, and load current. The closed-loop voltage-controlled model, described briefly in [17], includes two additional equations:

$$\dot{\langle\gamma\rangle}_0 = k_i\left(v_{ref} - \langle v_o\rangle_0\right) \tag{8}$$

$$\hat{d} = k_p\left(v_{ref} - \langle v_o\rangle_0\right) + \langle\gamma\rangle_0. \tag{9}$$

In the closed-loop model, the phase shift is generated internally by (9) and the input is replaced with voltage reference v_{ref}.

B. Origin of Steady-State Error

This section describes the origin of the large-signal modeling error. For simplicity, single phase shift modulation is considered in this discussion, since only one control variable is involved. The analysis applies equally to other modulation strategies.

The steady-state error manifests differently depending on how the model is used. If a phase shift is specified as an exogenous input (as is the case with the open-loop model), the error will affect the output voltage. If an output voltage and load current are specified, the error will affect the phase shift. Similarly, in a closed-loop operation, if a voltage reference and load current are specified, the phase shift will be affected.

For simplicity, we consider a lossless closed-loop converter with current source load (i.e., $R_t \to 0$, $R_{sh} \to \infty$) in a steady-state operation. The action of the controller forces output voltage to the voltage reference at a steady state, so the error will be restricted to the phase shift. The relationship in (1) reduces to $0 = i_t s_2(\tau, d) - i_L$, and the load current can be expanded as an infinite Fourier series as follows:

$$i_L = \sum_{k=-\infty}^{\infty} \langle i_t s_2(\tau, d)\rangle_k = \sum_{k=-\infty}^{\infty}\sum_{i=-\infty}^{\infty} \langle s_2(\tau, d)\rangle_{k-i}\langle i_t\rangle_i. \tag{10}$$

Considering only the dc average current, we have

$$\langle i_L\rangle_0 = \langle i_t s_2(\tau, d)\rangle_0 = \sum_{i=-\infty}^{\infty} \langle s_2(\tau, d)\rangle_{-i}\langle i_t\rangle_i. \tag{11}$$

Switching signal $s_2(\tau, d)$ is a phase-shifted square wave, and only has nonzero Fourier series coefficients at odd harmonics. The coefficients are functions of the phase shift, d:

$$\langle s_2(\tau, d)\rangle_k = \frac{-2\sin\pi k d}{k\pi} + j\frac{-2\cos\pi k d}{k\pi} \text{ for } k = 1, 3, \ldots \tag{12}$$

with $\langle s_2(\tau, d)\rangle_{-k} = \langle s_2(\tau, d)\rangle_k^*$. Note that this equation involves functions of d rather than $\hat{d}$, since the first harmonic approximation has not been applied to (1).

Under the same operating conditions, the dc average load current may be determined from the GAM state equations by simplifying and rearranging (5):

$$\begin{aligned}\langle i_L\rangle_0 &= \frac{-4\sin\pi\hat{d}}{\pi}\langle i_t\rangle_R + \frac{-4\cos\pi\hat{d}}{\pi}\langle i_t\rangle_I \\ &= \langle s_2(\tau, \hat{d})\rangle_{-1}\langle i_t\rangle_1 + \langle s_2(\tau, \hat{d})\rangle_1\langle i_t\rangle_{-1}.\end{aligned} \tag{13}$$

This expression corresponds exactly to the summation from (11) truncated after $i = \pm 1$, i.e., including the effect of the first harmonic approximation. The value of $\langle i_L\rangle_0$ must be the same in both (11) and (13), since it is specified as a constant, exogenous input. Therefore, the phase shift $\hat{d}$ that satisfies the equilibrium solution of the truncated model equations must be different from the real-world phase shift, d. This is consistent with the observations in both [11] and [16].

The preceding analysis shows that when the phase shift is treated as a free variable, a quantifiable difference exists between solutions to the GAM equations and steady-state expressions derived from first principles. In short, the objective of Section III-B is to eliminate the steady-state error by identifying and correcting for this difference.

III. Improved Model

This section describes the derivation of the improved DAB model, starting with an extension to more general modulation schemes. Following the derivation, Section III-B describes the large-signal error correction. In the interest of notational clarity, the angle-brackets used to denote averaging in the previous section are dropped for the remainder of the paper. The dc average of a generic variable x is therefore represented as x_0 rather than $\langle x\rangle_0$. Similarly, real and imaginary components of the fundamental harmonic are $x_R = \langle x\rangle_R$ and $x_I = \langle x\rangle_I$, respectively.

A. Modulation Scheme Extension

Applying the GAM framework to (1) and (2) yields the following:

$$\begin{aligned}\dot{v}_{o0} = &-\frac{1}{R_{sh}C_o}v_{o0} + \frac{1}{C_o}i_{t0}s_{20} + \frac{2}{C_o}i_{tR}s_{2R} \\ &+ \frac{2}{C_o}i_{tI}s_{2I} - \frac{1}{C_o}i_{L0}\end{aligned} \tag{14}$$

$$\begin{aligned}\dot{i}_{tR} = &\frac{1}{L_t}v_{\text{in}0}s_{1R} + \frac{1}{L_t}v_{\text{in}R}s_{10} - \frac{1}{L_t}v_{o0}s_{2R} \\ &- \frac{1}{L_t}v_{oR}s_{20} - \frac{R_t}{L_t}i_{tR} + \omega_s i_{tI}\end{aligned} \tag{15}$$

$$\begin{aligned}\dot{i}_{tI} = &\frac{1}{L_t}v_{\text{in}0}s_{1I} + \frac{1}{L_t}v_{\text{in}I}s_{10} - \frac{1}{L_t}v_{o0}s_{2I} \\ &- \frac{1}{L_t}v_{oI}s_{20} - \omega_s i_{tR} - \frac{R_t}{L_t}i_{tI}.\end{aligned} \tag{16}$$

To prevent saturation of the transformer, switching signals are typically defined such that their dc averages are zero, i.e., $s_{10} = s_{20} = 0$. Under this condition, the equations simplify as follows:

$$\dot{v}_{o0} = -\frac{1}{R_{sh}C_o}v_{o0} + \frac{2}{C_o}i_{tR}s_{2R} + \frac{2}{C_o}i_{tI}s_{2I} - \frac{1}{C_o}i_{L0} \tag{17}$$

$$\dot{i}_{tR} = \frac{1}{L_t}v_{\text{in}0}s_{1R} - \frac{1}{L_t}v_{o0}s_{2R} - \frac{R_t}{L_t}i_{tR} + \omega_s i_{tI} \tag{18}$$

$$\dot{i}_{tI} = \frac{1}{L_t}v_{\text{in}0}s_{1I} - \frac{1}{L_t}v_{o0}s_{2I} - \omega_s i_{tR} - \frac{R_t}{L_t}i_{tI}. \tag{19}$$

The preceding equations are applicable to any modulation strategy, provided that the dc average of the switching signals is zero. In the case of a triple phase shift modulation, the switching signals are functions of three control arguments: d_ϕ, d_p, and d_s.

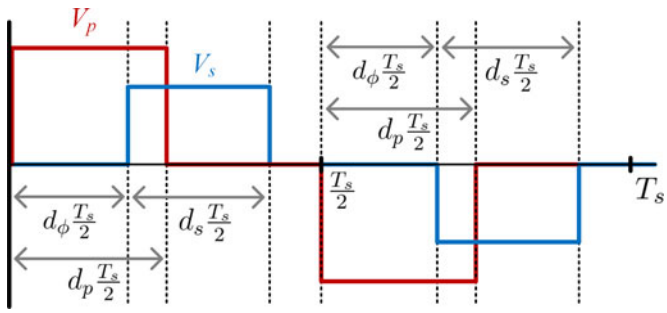

Fig. 2. Triple phase shift modulation scheme. V_p and V_s denote voltages applied to the primary and secondary windings of the transformer, respectively.

These variables are contained in vector $D = [d_\phi \quad d_p \quad d_s]^T$. The switching signals are as follows:

$$s_1(\tau, D) = \begin{cases} 1, & 0 \le \tau < \frac{d_p T_s}{2} \\ 0, & \frac{d_p T_s}{2} \le \tau < \frac{T_s}{2} \\ & \text{or } \frac{(1+d_p)T_s}{2} \le \tau < T_s \\ -1, & \frac{T_s}{2} \le \tau < \frac{(1+d_p)T_s}{2} \end{cases} \tag{20}$$

$$s_2(\tau, D) = \begin{cases} 1, & \frac{d_\phi T_s}{2} \le \tau < \frac{(d_s+d_\phi)T_s}{2} \\ & 0 \le \tau < \frac{d_\phi T_s}{2} \\ 0, & \text{or } \frac{(d_s+d_\phi)T_s}{2} \le \tau < \frac{(1+d_\phi)T_s}{2} \\ & \text{or } \frac{(1+d_s+d_\phi)T_s}{2} \le \tau < T_s \\ -1, & \frac{(1+d_\phi)T_s}{2} \le \tau < \frac{(1+d_s+d_\phi)T_s}{2}. \end{cases} \tag{21}$$

This switching scheme is very general; single, dual, and extended phase shift are special cases of the triple phase shift modulation [18]. A visual representation of the triple phase shift scheme is shown in Fig. 2. The three control variables describe the duty ratio of the voltages applied to the primary winding (d_p), secondary winding (d_s), and the phase shift between them (d_ϕ). An additional phase shift defined by the distance between the center points of the primary and secondary voltage pulses is d. This is an important parameter for describing triple phase shift operation [18], and is critical to the large-signal error correction method. It may be derived from the control variables as

$$d = d_\phi - \frac{d_p}{2} + \frac{d_s}{2}. \tag{22}$$

Switching signals for a dual phase shift modulation may be recovered by fixing $d_p = d_s$, and a single phase shift may be recovered by further constraining $d_p = d_s = 1$. In both of these cases, it is clear from (22) that $d = d_\phi$.

Taking the Fourier series of these signals, the real and imaginary components of the switching functions are as follows:

$$s_{1R}(D) = \frac{\sin(d_p \pi)}{\pi} \tag{23}$$

$$s_{1I}(D) = -\frac{2\sin\left(d_p \frac{\pi}{2}\right)^2}{\pi} \tag{24}$$

$$s_{2R}(D) = -\frac{\sin(d_\phi \pi) - \sin\left((d_s + d_\phi)\pi\right)}{\pi} \tag{25}$$

$$s_{2I}(D) = -\frac{\cos(d_\phi \pi) - \cos\left((d_s + d_\phi)\pi\right)}{\pi}. \tag{26}$$

Substituting the switching signal harmonic components above into state equations (17)–(19) produces a generalized average model for a DAB with triple phase shift modulation. Again, other modulation strategies can be recovered from these equations. For instance, applying the single phase shift condition ($d_p = d_s = 1$) in the general equations yields the original DAB model, i.e., (5)–(7).

B. Correction of Large-Signal Error

The second improvement involves correcting the large-signal modeling error due to the truncation of the Fourier series. In Section II-B, the error was discussed in terms of a difference between the exact phase shift, d, and the model phase shift, $\hat{d}$. The objective of the correction method is to include a description of the relationship between these two variables in the model framework, and use this expression to correct the large-signal error. This is done by introducing $\hat{d}$ in the model as an algebraic state. Adjusted control variables $\hat{D} = [\hat{d}_\phi \quad \hat{d}_p \quad \hat{d}_s]^T$ are derived from $\hat{d}$, and are used as arguments for the switching harmonic functions in (23)–(26). The evolution of $\hat{d}$ is governed by an algebraic equation that forces normalized power transfer expressions from the model to equal corresponding expressions derived from first principles.

The correction procedure is presented as follows. First, an expression for a normalized power transfer (in terms of $\hat{D}$) is derived from the GAM state equations. Next, corresponding expressions (in terms of D) from the existing literature are discussed. The difference between the two expressions is included in the final model as an algebraic constraint. Finally, the actual construction of $\hat{D}$ from $\hat{d}$ is described.

The correction factor is derived from lossless model equations, i.e., state equations with $R_t \to 0$. There are two reasons for this. First, for a well-designed transformer, R_t is small, and has little effect on the steady-state power transfer. An exception to this is the case of a single phase shift modulation, for which R_t plays a more significant role due to high circulating currents. This is considered in Section V. Second, the objective is to relate power relationships that are derived under the same conditions. Lossless power transfer equations are simple, and are readily available in the literature. Including the effect of R_t would involve a substantial increase in complexity, with only marginal benefit in terms of accuracy.

With $R_t \to 0$, a general power transfer expression is easily determined from the steady-state equations of the model. Equations (18) and (19) may be rearranged for i_{tI} and i_{tR}, respectively, and substituted into (17). The substitution results in

$$i_{L0} = \frac{2v_{\text{in}0}}{X_t}\left(s_{2R}s_{1I} - s_{1R}s_{2I}\right) \tag{27}$$

where $X_t = \omega_s L_t$ is the transformer reactance. All switching signal harmonics in (27)—and in all equations

TABLE I
TRIPLE PHASE SHIFT OPERATING MODES AND POWER TRANSFER EQUATIONS

Mode	Operating Region	Normalized Power Expression
I	$0 \le d \le \frac{d_s}{2} - \frac{d_p}{2}$	$P_N^* = \pi d_p \left(d_\phi - \frac{d_p}{2} - \frac{d_s}{2}\right)$
II	$0 \le d \le \frac{d_p}{2} - \frac{d_s}{2}$	$P_N^* = \pi d_s \left(d_\phi - \frac{d_p}{2} - \frac{d_s}{2}\right)$
III	$\left\lvert \frac{d_p}{2} - \frac{d_s}{2} \right\rvert \le d \le \min\left\{\frac{d_p}{2} + \frac{d_s}{2}, 1 - \frac{d_p}{2} - \frac{d_s}{2}\right\}$	$P_N^* = \frac{\pi}{2}\left(d_p(d_s + 2d_\phi) - d_p^2 - d_\phi^2\right)$
IV	$1 - \frac{d_p}{2} - \frac{d_s}{2} \le d \le \frac{d_p}{2} + \frac{d_s}{2}$	$P_N^* = \frac{\pi}{2}\left(2d_\phi(1 - d_\phi - d_s + d_p) + d_s(2 + d_p - d_s) - d_p^2 - 1\right)$
V	$\frac{d_p}{2} + \frac{d_s}{2} \le d \le 1 - \frac{d_p}{2} - \frac{d_s}{2}$	$P_N^* = \frac{\pi}{2} d_p d_s$

henceforth– - are functions of $\hat{D}$. The transferred power is then defined as follows:

$$P = v_{o0} i_{L0} = \frac{v_{\text{in}0} v_{o0}}{X_t} P_N \tag{28}$$

where P_N is the normalized power, and can be expressed as

$$P_N = 2\left(s_{2R} s_{1I} - s_{1R} s_{2I}\right). \tag{29}$$

Note that this formulation assumes a current source load, i.e., $R_{sh} \to \infty$, such that the dc average current through the secondary H-bridge is equal to the load current. This assumption serves only to prevent the need for an additional current term definition; including a finite resistive load term does not change the power transfer analysis.

Next, a steady-state power transfer equation must be determined using a method that does not include the first harmonic approximation. Suitable expressions are readily available in the literature, since power transfer equations are central to converter analysis. For instance, [18], [19], and [20] provide appropriate equations for triple, dual, and extended phase shift modulation, respectively. This function for power transfer is referred to as P^*, to distinguish from the expression determined from model equations.

Because of the wide range of operating cases that occur in triple phase shift modulation, no single expression for P^* is sufficient. In [18], five separate modes of operation are defined, each with their own power transfer expression. For full generality, P^* is defined as a piecewise function that selects between components according to the control inputs of the model. Table I shows the five power transfer equations and the operating conditions under which each is active. The active mode is determined by d, and is easily identified from the control inputs.

The expressions in Table I are the same as those in [18], but are given in the terminology used in this study, and are normalized as follows:

$$P^* = \frac{v_{\text{in}0} v_{o0}}{X_t} P_N^*. \tag{30}$$

The reason for this normalization is to simplify expressions when relating P^* to P. Clearly, when P^* and P are set equally, the leading fractional terms cancel out.

The final part of the correction procedure is determining how $\hat{D}$ is generated from $\hat{d}$. Because of the multiple degrees of freedom involved in the triple phase shift modulation, there are several viable ways to do this. The simplest method is to adjust only $\hat{d}_\phi$. The control variables are then

$$\hat{d}_\phi = \hat{d} + \frac{d_p}{2} - \frac{d_s}{2} \tag{31}$$

$$\hat{d}_p = d_p \tag{32}$$

$$\hat{d}_s = d_s. \tag{33}$$

This approach is sufficient for correcting error over the full possible range of control inputs for both the single and dual phase shift modulation.

For the triple phase shift modulation, an additional adjustment scheme is needed to ensure that a solution to the algebraic power equation exists over the entire operating space. For a solution to exist, the maximum normalized power transfer over the possible range of $\hat{d}$ must exceed the corresponding value of P^*. In addition to the correction applied to d_ϕ, an adjustment can be applied to d_p as

$$\hat{d}_\phi = d_\phi \tag{34}$$

$$\hat{d}_p = 2d_\phi - 2\hat{d} + d_s \tag{35}$$

$$\hat{d}_s = d_s. \tag{36}$$

For a given set of control inputs, the correction should be applied to either d_ϕ or d_p. The selection is made according to which choice produces the larger maximum normalized power transfer. This can be determined by the following condition:

$$\sin\left(\frac{d_p \pi}{2}\right) > \sin^2\left(\frac{\pi}{2}\left(\frac{d_s}{2} + d_\phi\right)\right). \tag{37}$$

If this condition is true, the correction should be applied to d_ϕ. If not, the correction should be applied to d_p. This condition may be derived as follows. First, analytical expressions for P_N as functions of $\hat{d}$ are determined for each of the correction schemes. This is done by substituting either (31), (32), and (33) or (34), (35), and (36) into (29). Next, the maximum values of the expressions for P_N are determined by setting derivatives with respect to $\hat{d}$ equal to 0, solving for $\hat{d}$, and substituting the results back into the P_N expressions. The right-hand and left-hand sides of (37) correspond to the two resultant expressions after common coefficients have been eliminated. Therefore, when the inequality is true, applying the correction through d_ϕ yields the higher maximum normalized power. This provides a simple method for identifying the proper correction scheme using only the control inputs to the model.

C. Model Organization

The structure of the proposed model framework is as follows:

$$\dot{x} = f(x, \hat{d}, u) \tag{38}$$

$$0 = g(x, \hat{d}, u) \tag{39}$$

where x is the state vector, u is the input vector, and $\hat{d}$ is an algebraic state variable. The model state equations are contained in the vector-valued function $f(\cdot)$. The scalar function $g(\cdot)$ is defined as

$$g(x, \hat{d}, u) \triangleq P^* - P. \tag{40}$$

Together, $f(\cdot)$ and $g(\cdot)$ define a semiexplicit (or type 1) system of differential algebraic equations (DAEs).

The state equations, state vector, and input vector differ according to whether an open- or closed-loop system is being modeled. Both are discussed below. Subscripts "o" and "c" are used to denote whether model elements (namely $f(\cdot)$, x, and u) pertain to the open-loop or closed-loop systems, respectively.

The state and input vectors of the open-loop model are as follows:

$$x_o = [v_{o0} \quad i_{tR} \quad i_{tI}]^T \tag{41}$$

$$u_o = [v_{\text{in}0} \quad i_{L0} \quad d_\phi \quad d_p \quad d_s]^T. \tag{42}$$

The state equations in $f_o(\cdot)$ are exactly those of the original DAB model, shown in Section II as (5)–(7). With respect to a large-signal error correction, the critical point of difference between this model and the model in [13] is that d, rather than $\hat{d}$, is defined as an input.

Triple phase shift modulation includes three control variables, and a wide variety of control structures and feedback mechanisms are possible. To limit the scope, the closed-loop formulation in the present study considers a single controller that regulates output voltage through the phase shift control variable, d_ϕ. The state and input vectors of the closed-loop model are as follows:

$$x_c = [v_{o0} \quad i_{tR} \quad i_{tI} \quad \gamma_0]^T \tag{43}$$

$$u_c = [v_{\text{in}0} \quad i_{L0} \quad v_{ref} \quad d_p \quad d_s]^T. \tag{44}$$

The additional state, γ_0, is contributed by the integral of a PI controller. In addition to the open-loop state equations, $f_c(\cdot)$ contains (8), which describes γ_0. In the original model, controller output was defined to be $\hat{d}_\phi$ (or, equivalently $\hat{d}$), as shown in (9). In contrast, controller output is defined in the present model as

$$d_\phi = k_p\left(v_{\text{ref}} - v_{o0}\right) + \gamma_0. \tag{45}$$

D. Discussion

The system defined by (38) and (39) is a large-signal generalized average model that is accurate in both transient and steady-state conditions. The model is a semiexplicit DAE system. Models of this type are commonly used for describing power systems [21] and are suitable for all applications expected of power electronics models. In particular, they may be used for time-domain simulations, stability analyses, or linearized to provide small-signal representations.

Both of the model improvements proposed here generalize the original DAB model from [13]. Extension to more advanced modulation strategies is a fairly straightforward improvement, but the inclusion of $g(\cdot)$, too, is a generalization of the original model. The model from [13] implicitly assumes that $\hat{d} = d$. This assumption may be included in the proposed modeling framework by defining $g(\cdot)$ as $0 = \hat{d} - d$. The resulting structure, when used with the single phase shift modulation, is identical to the model in [13].

While the general model is a DAE system, in some operating cases (namely, single phase shift modulation), it is possible to define $\hat{d}$ as an explicit function of d, i.e., by solving $g(\cdot)$ directly for $\hat{d}$. When an explicit solution is possible, the model may be converted into an equivalent system of ODEs.

In comparison to alternative continuous-time DAB modeling approaches, the primary advantage of the proposed modeling framework is its flexibility. The most closely related methods, i.e., [11] and [16], consider only the single phase shift modulation. The method in [11] is not affected by the large-signal error, but its derivation is inherently tied to the modulation strategy, meaning that new modulation schemes would require a full rederivation. In contrast, the proposed method is derived for general switching functions, so different modulation schemes are to be included by changing modular elements of the base model. Additionally, the method in [11] models the ac stage by deriving averaged equations for the dc currents into and out of the H-bridge circuits, effectively consolidating the switching circuit as a single averaged element. As a result, frequency domain accuracy is limited to one-tenth of the switching frequency. In contrast, the original DAB model from [13] is accurate up to one-third of the switching frequency. The upper frequency bound is, in general, imposed by the eigenvalues of the dynamic model [10], [22]. The proposed model maintains the small-signal accuracy of the model from [13]; when linearized, the eigenvalues of the proposed model are very close to those of the original model, meaning their upper limits are similar as well. This is further illustrated in Section VI.

The method from [16] is more closely related to the proposed framework than [11], but differs in how the correction factor is applied. The correction factor in [16] modifies the load and state variables directly, and the modifications required are different for each of the state variables. In this study, error correction is applied through an algebraic equation rather than through the model state variables, so modifications to the correction factor equation do not change the base model. This makes it possible to include more general modulation strategies or lossy correction factors within the same modeling framework.

IV. Partial Derivatives and Small-Signal Models

Partial derivatives are central to many modeling applications. Partial derivatives are used for calculating steady-state solutions to model equations, time-domain simulation via numerical integration, and linearization for small-signal analysis. The partial derivatives of the models under consideration are given in this section.

A. Open-Loop System

The partial derivatives of the open-loop model equations with respect to converter states are as follows:

$$\frac{\partial f_o}{\partial x_o} = \begin{bmatrix} \frac{-1}{R_{sh}C_o} & \frac{2}{C_o}s_{2R} & \frac{2}{C_o}s_{2I} \\ \frac{-1}{L_t}s_{2R} & \frac{-R_t}{L_t} & \omega_s \\ \frac{-1}{L_t}s_{2I} & -\omega_s & \frac{-R_t}{L_t} \end{bmatrix} \tag{46}$$

$$\frac{\partial f_o}{\partial \hat{d}} = \begin{bmatrix} \frac{2}{C_o}\left(i_{tR}\frac{\partial s_{2R}}{\partial \hat{d}} + i_{tI}\frac{\partial s_{2I}}{\partial \hat{d}}\right) \\ \frac{1}{L_t}\left(v_{\text{in}0}\frac{\partial s_{1R}}{\partial \hat{d}} - v_{o0}\frac{\partial s_{2R}}{\partial \hat{d}}\right) \\ \frac{1}{L_t}\left(v_{\text{in}0}\frac{\partial s_{1I}}{\partial \hat{d}} - v_{o0}\frac{\partial s_{2I}}{\partial \hat{d}}\right) \end{bmatrix}. \tag{47}$$

Derivatives with respect to inputs are given in (48) shown at the bottom of this page.

The switching signal derivatives are shown in general form in these equations. The specific derivatives for the triple phase shift modulation are given in Section IV-C.

The partial derivatives of the algebraic function $g(\cdot)$ are as follows:

$$\frac{\partial g}{\partial x_o} = \begin{bmatrix} 0 & 0 & 0 \end{bmatrix} \tag{49}$$

$$\frac{\partial g}{\partial \hat{d}} = 2\left(s_{1R}\frac{\partial s_{2I}}{\partial \hat{d}} + s_{2I}\frac{\partial s_{1R}}{\partial \hat{d}}\right) - 2\left(s_{2R}\frac{\partial s_{1I}}{\partial \hat{d}} + s_{1I}\frac{\partial s_{2R}}{\partial \hat{d}}\right) \tag{50}$$

$$\frac{\partial g}{\partial u_o} = \begin{bmatrix} 0 & 0 & \frac{\partial g}{\partial d_\phi} & \frac{\partial g}{\partial d_p} & \frac{\partial g}{\partial d_s} \end{bmatrix} \tag{51}$$

where $\frac{\partial g}{\partial d_\phi}$, $\frac{\partial g}{\partial d_p}$, and $\frac{\partial g}{\partial d_s}$ are given by

$$\frac{\partial g}{\partial d_\phi} = \frac{\partial P_N^*}{\partial d_\phi} + 2\left(s_{1R}\frac{\partial s_{2I}}{\partial d_\phi} + s_{2I}\frac{\partial s_{1R}}{\partial d_\phi}\right) - 2\left(s_{2R}\frac{\partial s_{1I}}{\partial d_\phi} + s_{1I}\frac{\partial s_{2R}}{\partial d_\phi}\right) \tag{52}$$

$$\frac{\partial g}{\partial d_p} = \frac{\partial P_N^*}{\partial d_p} + 2\left(s_{1R}\frac{\partial s_{2I}}{\partial d_p} + s_{2I}\frac{\partial s_{1R}}{\partial d_p}\right) - 2\left(s_{2R}\frac{\partial s_{1I}}{\partial d_p} + s_{1I}\frac{\partial s_{2R}}{\partial d_p}\right) \tag{53}$$

$$\frac{\partial g}{\partial d_s} = \frac{\partial P_N^*}{\partial d_s} + 2\left(s_{1R}\frac{\partial s_{2I}}{\partial d_s} + s_{2I}\frac{\partial s_{1R}}{\partial d_s}\right) - 2\left(s_{2R}\frac{\partial s_{1I}}{\partial d_s} + s_{1I}\frac{\partial s_{2R}}{\partial d_s}\right). \tag{54}$$

The derivatives of P_N^* with respect to control inputs depend on the operational mode. For all of the cases shown in Table I, these terms are straightforward derivatives of polynomial functions.

B. Closed-Loop System

The partial derivatives of the closed-loop model equations are as follows:

$$\frac{\partial f_c}{\partial x_c} = \begin{bmatrix} \frac{-1}{R_{sh}C_o} & \frac{2}{C_o}s_{2R} & \frac{2}{C_o}s_{2I} & 0 \\ \frac{-1}{L_t}s_{2R} & \frac{-R_t}{L_t} & \omega_s & 0 \\ \frac{-1}{L_t}s_{2I} & -\omega_s & \frac{-R_t}{L_t} & 0 \\ -k_i & 0 & 0 & 0 \end{bmatrix} \tag{55}$$

$$\frac{\partial f_c}{\partial \hat{d}_\phi} = \begin{bmatrix} \frac{\partial f_o}{\partial \hat{d}_\phi} \\ 0 \end{bmatrix} \tag{56}$$

where $\frac{\partial f_o}{\partial \hat{d}_\phi}$ is given in (47). Derivative $\frac{\partial f_c}{\partial u_c}$ is given in (57) shown at the bottom of this page. The derivative of $g(\cdot)$ with respect to $\hat{d}_\phi$ is the same as for the open-loop system, as shown in (50). The remaining derivatives of $g(\cdot)$ are as follows:

$$\frac{\partial g}{\partial x_c} = \begin{bmatrix} -k_p\frac{\partial P_N^*}{\partial d_\phi} & 0 & 0 & \frac{\partial P_N^*}{\partial d_\phi} \end{bmatrix} \tag{58}$$

$$\frac{\partial g}{\partial u_c} = \begin{bmatrix} 0 & 0 & k_p\frac{\partial g}{\partial d_\phi} & \frac{\partial g}{\partial d_p} & \frac{\partial g}{\partial d_s} \end{bmatrix} \tag{59}$$

where $\frac{\partial g}{\partial d_\phi}$, $\frac{\partial g}{\partial d_p}$, and $\frac{\partial g}{\partial d_s}$ are given (52)–(54), respectively.

C. Switching Signal Derivatives

When the correction factor is applied through d_ϕ, switching function s_1 is only a function of control variable d_p. Therefore, the partial derivatives of s_{1R} and s_{1I} with respect to $\hat{d}$, d_ϕ, and d_s are 0. The derivatives with respect to d_p are as follows:

$$\frac{\partial s_{1R}}{\partial d_p} = \cos(d_p\pi) \tag{60}$$

$$\frac{\partial s_{1I}}{\partial d_p} = -\sin(d_p\pi). \tag{61}$$

$$\frac{\partial f_o}{\partial u_o} = \begin{bmatrix} 0 & \frac{-1}{C_o} & \frac{2}{C_o}\left(i_{tR}\frac{\partial s_{2R}}{\partial d_\phi} + i_{tI}\frac{\partial s_{2I}}{\partial d_\phi}\right) & \frac{2}{C_o}\left(i_{tR}\frac{\partial s_{2R}}{\partial d_p} + i_{tI}\frac{\partial s_{2I}}{\partial d_p}\right) & \frac{2}{C_o}\left(i_{tR}\frac{\partial s_{2R}}{\partial d_s} + i_{tI}\frac{\partial s_{2I}}{\partial d_s}\right) \\ \frac{1}{L_t}s_{1R} & 0 & \frac{1}{L_t}\left(v_{\text{in}0}\frac{\partial s_{1R}}{\partial d_\phi} - v_{o0}\frac{\partial s_{2R}}{\partial d_\phi}\right) & \frac{1}{L_t}\left(v_{\text{in}0}\frac{\partial s_{1R}}{\partial d_p} - v_{o0}\frac{\partial s_{2R}}{\partial d_p}\right) & \frac{1}{L_t}\left(v_{\text{in}0}\frac{\partial s_{1R}}{\partial d_s} - v_{o0}\frac{\partial s_{2R}}{\partial d_s}\right) \\ \frac{1}{L_t}s_{1I} & 0 & \frac{1}{L_t}\left(v_{\text{in}0}\frac{\partial s_{1I}}{\partial d_\phi} - v_{o0}\frac{\partial s_{2I}}{\partial d_\phi}\right) & \frac{1}{L_t}\left(v_{\text{in}0}\frac{\partial s_{1I}}{\partial d_p} - v_{o0}\frac{\partial s_{2I}}{\partial d_p}\right) & \frac{1}{L_t}\left(v_{\text{in}0}\frac{\partial s_{1I}}{\partial d_s} - v_{o0}\frac{\partial s_{2I}}{\partial d_s}\right) \end{bmatrix} \tag{48}$$

$$\frac{\partial f_c}{\partial u_c} = \begin{bmatrix} 0 & \frac{-1}{C_o} & 0 & \frac{2}{C_o}\left(i_{tR}\frac{\partial s_{2R}}{\partial d_p} + i_{tI}\frac{\partial s_{2I}}{\partial d_p}\right) & \frac{2}{C_o}\left(i_{tR}\frac{\partial s_{2R}}{\partial d_s} + i_{tI}\frac{\partial s_{2I}}{\partial d_s}\right) \\ \frac{1}{L_t}s_{1R} & 0 & 0 & \frac{1}{L_t}\left(v_{\text{in}0}\frac{\partial s_{1R}}{\partial d_p} - v_{o0}\frac{\partial s_{2R}}{\partial d_p}\right) & \frac{1}{L_t}\left(v_{\text{in}0}\frac{\partial s_{1R}}{\partial d_s} - v_{o0}\frac{\partial s_{2R}}{\partial d_s}\right) \\ \frac{1}{L_t}s_{1I} & 0 & 0 & \frac{1}{L_t}\left(v_{\text{in}0}\frac{\partial s_{1I}}{\partial d_p} - v_{o0}\frac{\partial s_{2I}}{\partial d_p}\right) & \frac{1}{L_t}\left(v_{\text{in}0}\frac{\partial s_{1I}}{\partial d_s} - v_{o0}\frac{\partial s_{2I}}{\partial d_s}\right) \\ 0 & 0 & k_i & 0 & 0 \end{bmatrix} \tag{57}$$

Switching function s_2 is a function of variables $\hat{d}$ (through $\hat{d}_\phi$), d_p, and d_s. Since d_ϕ is replaced, the derivatives with respect to d_ϕ are 0. The remaining derivatives are as follows:

$$\frac{\partial s_{2R}}{\partial d_p} = \frac{1}{2}\left(\cos((d_s + \hat{d}_\phi)\pi) - \cos(\hat{d}_\phi \pi)\right) \tag{62}$$

$$\frac{\partial s_{2I}}{\partial d_p} = \frac{1}{2}\left(\sin(\hat{d}_\phi \pi) - \sin((d_s + \hat{d}_\phi)\pi)\right) \tag{63}$$

$$\frac{\partial s_{2R}}{\partial d_s} = \frac{1}{2}\left(\cos((d_s + \hat{d}_\phi)\pi) + \cos(\hat{d}_\phi \pi)\right) \tag{64}$$

$$\frac{\partial s_{2I}}{\partial d_s} = \frac{-1}{2}\left(\sin(\hat{d}_\phi \pi) + \sin((d_s + \hat{d}_\phi)\pi)\right) \tag{65}$$

$$\frac{\partial s_{2R}}{\partial \hat{d}} = \cos((d_s + \hat{d}_\phi)\pi) - \cos(\hat{d}_\phi \pi) \tag{66}$$

$$\frac{\partial s_{2I}}{\partial \hat{d}} = \sin(\hat{d}_\phi \pi) - \sin((d_s + \hat{d}_\phi)\pi). \tag{67}$$

When the correction factor is applied through d_p, switching function s_1 depends on $\hat{d}$ (through $\hat{d}_p$), d_s, and d_ϕ. Input d_1 is replaced, so derivatives with respect to d_1 are 0:

$$\frac{\partial s_{1R}}{\partial d_\phi} = \cos(\hat{d}_p \pi) \tag{68}$$

$$\frac{\partial s_{1I}}{\partial d_\phi} = -\sin(\hat{d}_p \pi) \tag{69}$$

$$\frac{\partial s_{1R}}{\partial d_s} = 2\cos(\hat{d}_p \pi) \tag{70}$$

$$\frac{\partial s_{1I}}{\partial d_s} = -2\sin(\hat{d}_p \pi) \tag{71}$$

$$\frac{\partial s_{1R}}{\partial \hat{d}} = -2\cos(\hat{d}_p \pi) \tag{72}$$

$$\frac{\partial s_{1I}}{\partial \hat{d}} = 2\sin(\hat{d}_p \pi). \tag{73}$$

Finally, switching function s_2 depends only on d_ϕ and d_s, so derivatives with respect to d_p and $\hat{d}$ are zero:

$$\frac{\partial s_{2R}}{\partial d_\phi} = \cos((d_s + d_\phi)\pi) \tag{74}$$

$$\frac{\partial s_{2I}}{\partial d_\phi} = -\sin((d_s + d_\phi)\pi) \tag{75}$$

$$\frac{\partial s_{2R}}{\partial d_s} = \cos((d_s + d_\phi)\pi) - \cos(d_\phi \pi) \tag{76}$$

$$\frac{\partial s_{2I}}{\partial d_s} = \sin(d_\phi \pi) - \sin((d_s + d_\phi)\pi). \tag{77}$$

D. Small-Signal Models

For all models under consideration, the small-signal models have the form

$$\dot{\tilde{x}} = A\tilde{x} + B\tilde{u} \tag{78}$$

where $\tilde{x}$ is a vector of small-signal deviations around a steady-state operating point. Matrices A and B are calculated using matrix operations, given here in terms of generic functions $f(\cdot)$ and $g(\cdot)$ as follows:

$$A = \frac{\partial f}{\partial x} - \frac{\partial f}{\partial \hat{d}}\left(\frac{\partial g}{\partial \hat{d}}\right)^{-1}\frac{\partial g}{\partial x} \tag{79}$$

$$B = \frac{\partial f}{\partial u} - \frac{\partial f}{\partial \hat{d}}\left(\frac{\partial g}{\partial \hat{d}}\right)^{-1}\frac{\partial g}{\partial u}. \tag{80}$$

The derivation for these linearized matrices is given in the Appendix.

V. Considerations for the Single Phase Shift Modulation

Although the single phase shift modulation has several performance deficiencies, it is still commonly used in the DAB literature due to its overall simplicity. In particular, single phase shift is commonly used in studies that include DAB converters as elements of a larger system [15], [23]. In light of this, a more detailed consideration of the single phase shift case is given here. As a secondary benefit, this section provides a simple illustration of how the general framework outlined in Section III may be applied to a specific modulation scheme.

A. Model Simplifications

Single phase shift modulation is a subset of a triple phase shift, and corresponds to the case in which d_p and d_s are constant and equal to 1. This condition simplifies the model. With d_p and d_s fixed, it is not necessary to include these variables as model inputs, and $d_\phi = d$.

The first harmonic components of switching functions for the single phase shift modulation may be recovered by fixing $d_p = d_s = 1$ in (23)–(26):

$$s_{1R}(\hat{d}) = 0 \tag{81}$$

$$s_{1I}(\hat{d}) = -\frac{2}{\pi} \tag{82}$$

$$s_{2R}(\hat{d}) = -\frac{2\sin(\hat{d}\pi)}{\pi} \tag{83}$$

$$s_{2I}(\hat{d}) = -\frac{2\cos(\hat{d}\pi)}{\pi}. \tag{84}$$

Furthermore, the single phase shift modulation restricts the operating region of the converter. According to Table I, single phase shift modulation is entirely contained in Mode IV, so only one power transfer equation is necessary.

B. Lossless Case

Without including R_t, the procedure begins directly with a normalized power:

$$P_N = 2(s_{2R}s_{1I} - s_{1R}s_{2I}) = \frac{8\sin(\hat{d}\pi)}{\pi^2}. \tag{85}$$

Next, the power transfer equation from Table I is reduced using the same conditions on d_p and d_s. These conditions restrict the operating region to Mode IV, and the corresponding equation

simplifies to

$$P_N^* = \pi d(1-d). \tag{86}$$

Therefore, the equation that relates $\hat{d}$ to d is

$$g(x, \hat{d}, u) = \frac{\pi^3 d(1-d)}{8} - \sin \pi \hat{d}. \tag{87}$$

C. Lossy Case

In the lossy case, R_t is nonzero. The parameter R_t represents winding losses in the transformer, but it can also be used as a lumped-element parameter to represent conduction losses in the semiconductors as well. Including R_t in the large-signal error correction requires a substantial increase in the complexity, and is only necessary when the losses modeled by R_t become significant. One case in which R_t plays an important role is the single phase shift modulation with high phase shift values. Under these conditions, the transformer will experience high circulating currents, and conduction losses will be larger. While this issue may be addressed through the use of more advanced modulation schemes, there is still a need to accurately represent converter behavior under these conditions when the single phase shift modulation is used.

The problem with including R_t in the error correction is that the power transfer equations become dependent on state variables and hardware parameters. In the previous cases, $g(\cdot)$ was only dependent on control variables. This is not the case when R_t is included. Nevertheless, the procedure for deriving the correction equation remains the same.

The expression for i_{L0} in terms of $\hat{d}$ given in (27) is derived with $R_t \to 0$. Applying the same derivation procedure, i.e., solving the state equations with time derivatives set to 0, a similar expression may be derived with R_t included. In general form, the resulting expression is as follows:

$$\begin{aligned} i_{L0} = \frac{2}{R_t^2 + X_t^2} &\left[(s_{2R} R_t - s_{2I} X_t)(v_{\text{in}0} s_{1R} - v_{o0} s_{2R}) \right. \\ &\left. + (s_{2I} R_t + s_{2R} X_t)(v_{\text{in}0} s_{1I} - v_{o0} s_{2I}) \right]. \end{aligned} \tag{88}$$

After applying the simplifications for the single phase shift modulation, this may be more conveniently written as follows:

$$i_{L0} = \frac{2X_t}{\pi R_t^2 K}(v_{\text{in}0} R_t \cos \pi \hat{d} + v_{\text{in}0} X_t \sin \pi \hat{d} - v_{o0} R_t) \tag{89}$$

where K is a hardware constant given by

$$K = \frac{\pi}{4} \frac{X_t (R_t^2 + X_t^2)}{R_t^2}. \tag{90}$$

The definition of K is arbitrary at this point, but substantially simplifies derivative terms when linearizing the model.

The next step is to determine a corresponding expression in terms of d. Average output current equations have previously been derived in the literature. One such equation is used by the average value model proposed in [11]. However, the equation in question (see [11, Eq. (19)]) is valid only for a unidirectional power flow, i.e., $d > 0$. A more suitable equation is derived in [12] by integrating the instantaneous current terms, which are piecewise exponential, over the switching period. This expression (originally [12, Eq. (6)]) is cumbersome; Zhang *et al.* [12] spent considerable effort obtaining a more manageable approximation. In this study, we use a simplified form of the exact equation:

$$\begin{aligned} i_{L0}^* = &\frac{(v_{\text{in}0} - v_{o0})}{R_t} + \frac{v_{o0}}{\theta R_t} \tanh \theta \\ &+ \frac{d}{|d|}\left(\frac{v_{\text{in}0}}{\theta R_t}\right)\left[1 - 2\theta d - \operatorname{sech} \theta \exp\left(\frac{d}{|d|}\theta - 2\theta d\right)\right] \end{aligned} \tag{91}$$

where θ is a hardware constant:

$$\theta = \frac{\pi R_t}{2X_t}. \tag{92}$$

The expression in (91) is mathematically equivalent to [12, Eq. (6)]. The only differences are that notational conventions have been changed (e.g., phase shift is defined as a fraction of the switching period rather than an angle) and simplifications have been applied using hyperbolic function identities. The exact conversion consists entirely of standard algebraic manipulations, and the result is easily verified using a computer algebra system.

The form of (91) is relatively simple. The arguments of hyperbolic functions $\tanh$ and sech are hardware constants, hence they have very little impact on the complexity when applied in the model. Furthermore, the sign factors $\frac{d}{|d|}$ are only necessary to support bidirectional operation. For the unidirectional power flow case, these may be eliminated entirely.

The final step is to form the algebraic correction equation. Since $P = v_{o0} i_{L0}$ and $P^* = v_{o0} i_{L0}^*$, the equation may be defined as

$$\begin{aligned} g(x, \hat{d}, u) &= i_{L0}^* - i_{L0} \\ &= -v_{\text{in}0} R_t \cos \pi \hat{d} - v_{\text{in}0} X_t \sin \pi \hat{d} + v_{o0} R_t \\ &\quad + K(v_{\text{in}0} - v_{o0})\theta + K v_{o0} \tanh \theta \\ &\quad + K v_{\text{in}0} \frac{d}{|d|}\left(1 - 2\theta d - \operatorname{sech} \theta \exp\left(\frac{d}{|d|}\theta - 2\theta d\right)\right). \end{aligned} \tag{93}$$

Since (93) includes v_{o0} and $v_{\text{in}0}$, some of the derivatives from Section IV must be changed. For the open-loop system, the derivatives of $g(\cdot)$ are as follows:

$$\frac{\partial g}{\partial x_o} = \begin{bmatrix} R_t - K(\theta - \tanh \theta) & 0 & 0 \end{bmatrix} \tag{94}$$

$$\frac{\partial g}{\partial \hat{d}} = \pi v_{\text{in}0}\left(R_t \sin \pi \hat{d} - X_t \cos \pi \hat{d}\right) \tag{95}$$

$$\frac{\partial g}{\partial u_o} = \begin{bmatrix} \frac{\partial g}{\partial v_{\text{in}0}} & 0 & \frac{\partial g}{\partial d} \end{bmatrix} \tag{96}$$

where elements $\frac{\partial g}{\partial v_{\text{in}0}}$ and $\frac{\partial g}{\partial d}$ are given by

$$\begin{aligned} \frac{\partial g}{\partial v_{\text{in}0}} = &K \frac{d}{|d|}\left(1 - 2\theta d - \operatorname{sech} \theta \exp\left(\frac{d}{|d|}\theta - 2\theta d\right)\right) \\ &+ K\theta - R_t \cos \pi \hat{d} - X_t \sin \pi \hat{d} \end{aligned} \tag{97}$$

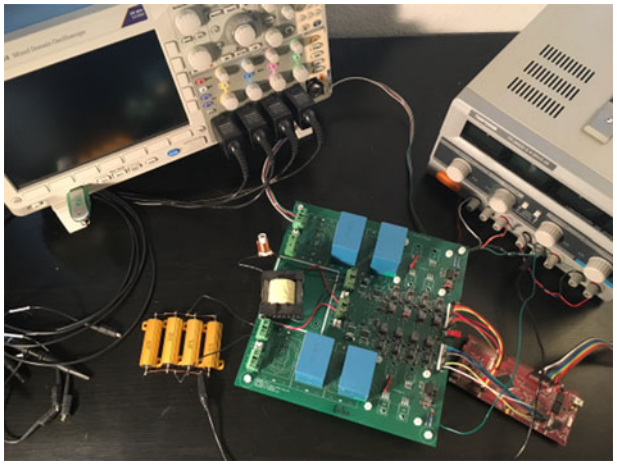

Fig. 3. Prototype DAB converter.

TABLE II
CONTROL AND HARDWARE PARAMETERS

Parameter	Value	Parameter	Value
C_{in}	40 μF	C_o	40 μF
L_t	5.53 μH	R_t	0.55 Ω
$n_1 : n_2$	1 : 0.85	R_{sh}	6.667 Ω
k_p	0.01	k_i	25

$$\frac{\partial g}{\partial d} = \left(\frac{2d\theta K v_{\text{in}0}}{|d|}\right)\left(\operatorname{sech}\theta \exp\left(\frac{d}{|d|}\theta - 2\theta d\right) - 1\right). \tag{98}$$

For the closed-loop system, the derivatives of $g(\cdot)$ are as follows:

$$\frac{\partial g}{\partial x_c} = \left[\, R_t - K\left(\theta - \tanh\theta\right) \quad 0 \quad 0 \quad \tfrac{\partial g}{\partial d} \,\right] \tag{99}$$

$$\frac{\partial g}{\partial u_c} = \left[\, \tfrac{\partial g}{\partial v_{\text{in}0}} \quad 0 \quad k_p \tfrac{\partial g}{\partial d} \,\right] \tag{100}$$

where the elements $\frac{\partial g}{\partial v_{\text{in}0}}$ and $\frac{\partial g}{\partial d}$ are given in (97) and (98), respectively.

VI. VERIFICATION

To validate the proposed models, experiments were performed to verify model accuracy both at the steady state and during transient response. The experiments were conducted using a small-scale DAB prototype, shown in Fig. 3. Switching simulations performed in PLECS supplement the hardware results. The prototype converter is controlled by a Texas Instruments TMS320F28377S digital signal processor (DSP). Both the sampling rate and switching frequency of the converter were 80 kHz. The switching deadtime was $t_d = 300$ ns. These and other important parameters are given in Table II.

The effect of the switching deadtime on the converter behavior is significant in practice. Deadtime introduces conduction modes that are not explicitly included in the model derivation, and effectively changes the control inputs d_ϕ, d_p, and d_s [24].

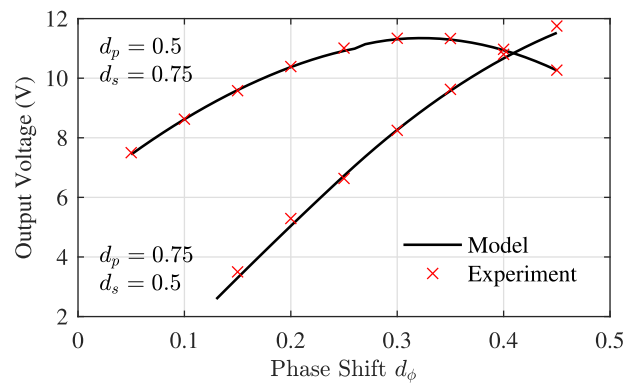

Fig. 4. Comparison of relationships between phase shift inputs and output voltage for the triple phase shift modulation.

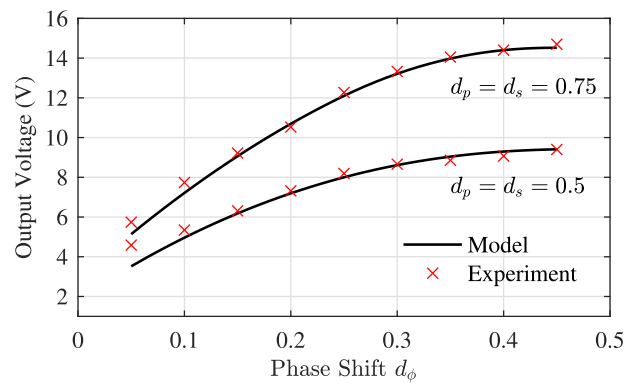

Fig. 5. Comparison of relationships between phase shift inputs and output voltage for the dual phase shift modulation.

Including conduction modes related to deadtime in the model would require a substantial increase in complexity. Alternatively, deadtime compensation strategies may be employed in the control system. The latter approach is used here: deadtime is compensated in the controller by applying phase shift corrections according to [25].

A. Steady-State Accuracy

The first test considers the steady-state accuracy. The converter output voltage is measured while varying d_ϕ. A resistive load is used and input voltage is fixed at 10 V throughout. Results for triple and dual phase shift modulation are shown in Figs. 4 and 5, respectively. For these results, and the dual and triple phase shift dynamic results in the following section, lossless model correction factors have been used. Two combinations of d_p and d_s are considered in each plot. Fig. 4 shows results with $d_p = 0.5$, $d_s = 0.75$ and $d_p = 0.75$, $d_s = 0.5$. Fig. 4 shows results with $d_p = d_s = 0.5$ and $d_p = d_s = 0.75$. In all cases, d_ϕ varies over the operating range for which $0 < d < 0.5$. The results indicate that the large-signal model accurately predicts the steady-state response of the converter.

Results for the single phase shift modulation are shown in Fig. 6. In this case, the hardware results are compared to the uncorrected model and to the corrected model using both

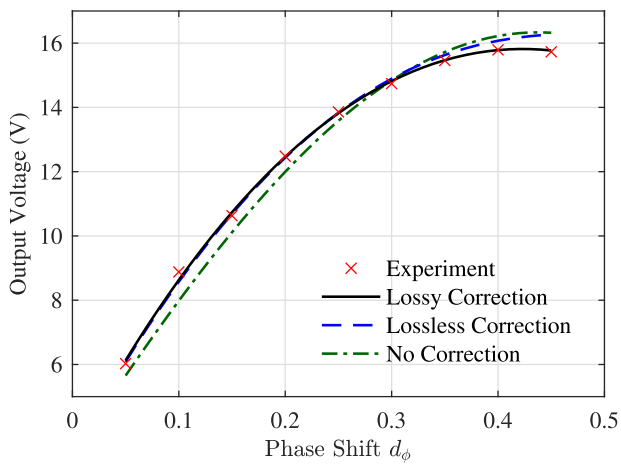

Fig. 6. Comparison of relationships between the phase shift and output voltage for the single phase shift modulation.

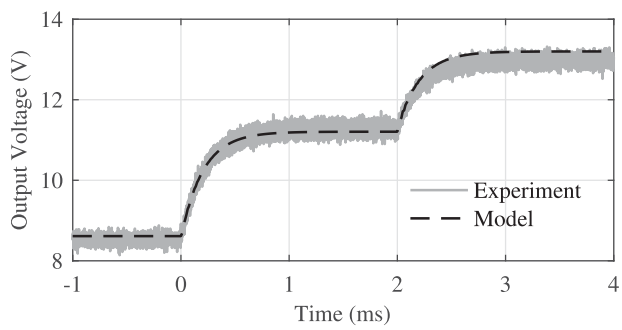

Fig. 7. Open-loop voltage transient response for step changes in control inputs for the triple phase shift modulation. At $t = 0$ ms, d_s changes from 0.5 to 0.75; at $t = 2$ ms, d_p changes from 0.5 to 0.75.

lossless and lossy correction factors. As expected, the lossy variant is more accurate for larger phase shifts, since the effects of converter loss become more significant.

B. Dynamic Accuracy

The second set of tests consider dynamic response, namely the output voltage transients for step changes in phase shift inputs. The experiment uses same the resistive load and 10 V input voltage as in the previous test. For the triple phase shift modulation, step changes to d_p and d_s are considered. The results are shown in Fig. 7. At the start of the experiment, both d_p and d_s are 0.5; at $t = 0$ ms, d_s steps from 0.5 to 0.75. At $t = 2$ ms, d_p steps from 0.5 to 0.75. The model predictions and experimental results are consistent for both transients.

In the dual phase shift modulation, d_p and d_s are equal, so only one step change is considered. The results for the dual phase shift modulation are shown in Fig. 8. At time $t = 0$ ms, both d_p and d_s change from 0.5 to 0.75. Again, the model accurately predicts the response.

For the single phase shift, step changes in d_ϕ are considered. As in the steady-state experiments, hardware measurements are compared to the uncorrected model and to both lossless and

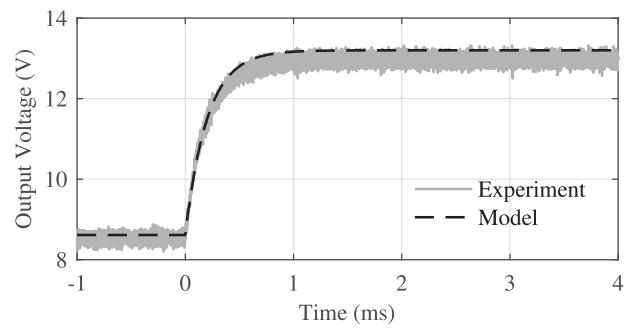

Fig. 8. Open-loop voltage transient response for step changes in control inputs for dual phase shift modulation. At $t = 0$ ms d_p (and d_s) changes from 0.5 to 0.75.

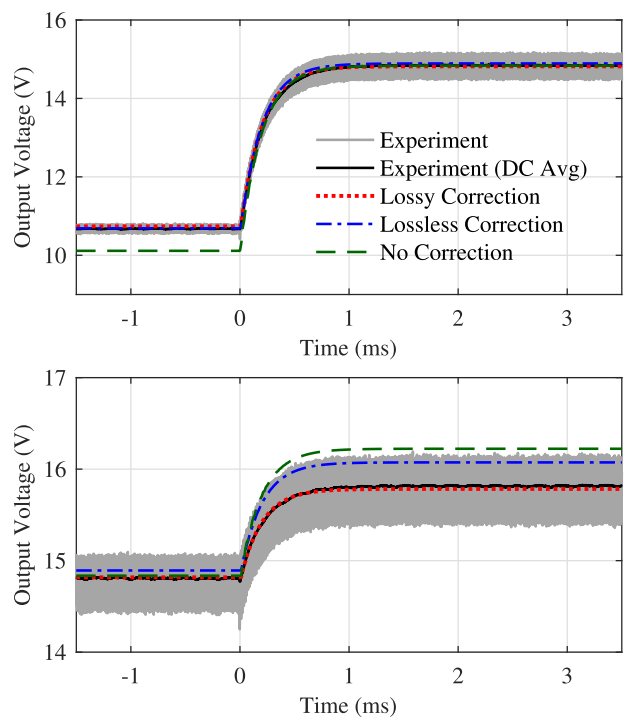

Fig. 9. Open-loop voltage transient response for step changes in phase shift. At $t = 0$ ms, d changes from 0.15 to 0.3 (top) and from 0.3 to 0.4 (bottom). Experimental results are shown as raw measurements and the dc average over a single switching period.

lossy variants of the corrected model. The results are shown in Fig. 9. In the top plot, d_ϕ steps from 0.15 to 0.3 at $t = 0$ ms; in the bottom plot, d_ϕ steps from 0.3 to 0.4. The plots show both the raw hardware measurements and dc sliding averages of the measurements, taken over a single switching period. These averages are, by definition, the experimental v_{o0}.

The top plots of Fig. 9 show that if large phase shifts are avoided, the difference in the accuracy between the lossless and lossy model variants is negligible. However, the bottom plots show a situation in which the lossy correction equation is measurably superior. This is particularly clear when comparing model predictions to the dc average output voltage measurements. In both cases, the inclusion of either correction factor consistently improves the accuracy with respect to the uncorrected model.

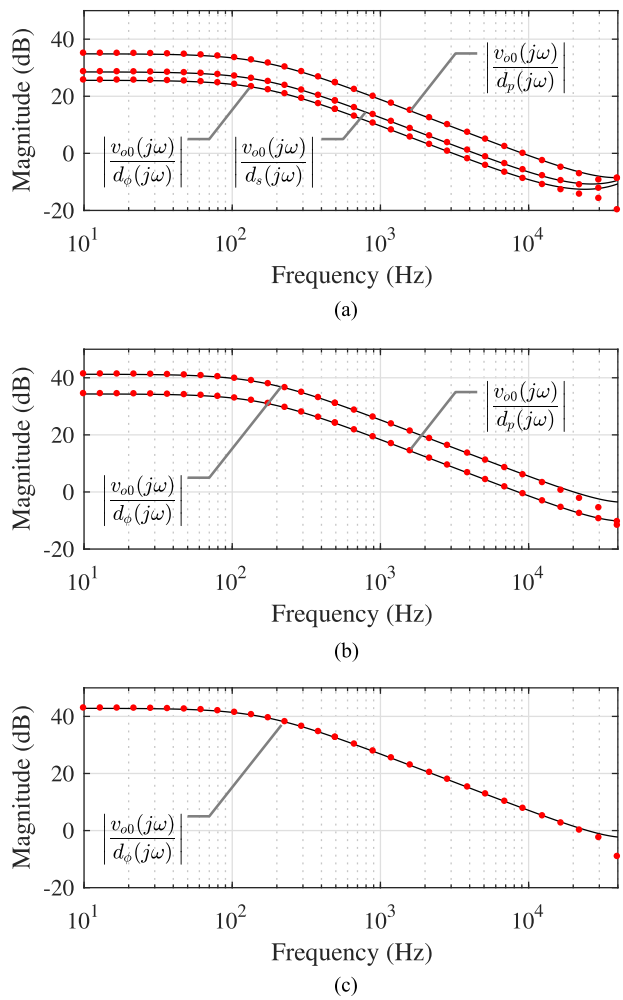

Fig. 10. Magnitude responses of control-to-output transfer functions. Model predictions are shown as solid lines, dots indicate results of switching simulations. (a) TPS control-to-output transfer functions. (b) DPS control-to-output transfer functions. (c) SPS control-to-output transfer function.

TABLE III
SIMULATION PARAMETERS

Parameter	Value	Parameter	Value
C_{in}	40 μF	C_o	200 μF
L_t	4 μH	R_t	0.01 Ω
$n_1 : n_2$	1 : 1	R_{sh}	5 Ω
v_{in}	30 V	i_{L0}	2 A

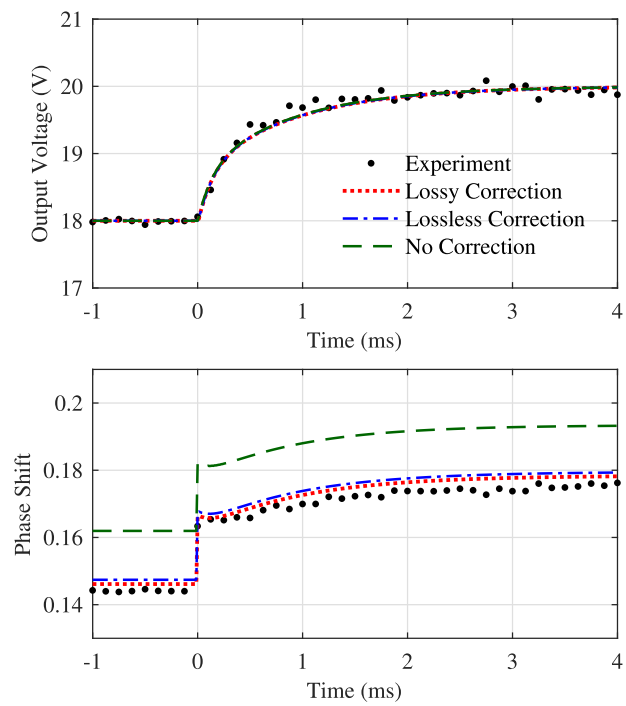

Fig. 11. Closed-loop transient response for step change reference voltage. At $t = 0$ ms, v_{ref} changes from 18 to 20 V. Plots show output voltage (top) and closed-loop phase shift (bottom).

The results in Fig. 9 show that the proposed modeling framework improves on the accuracy of the original model. However, these results use large-signal model predictions. To assess the small-signal accuracy of the models, frequency-domain predictions are compared to ac sweep analyses from switching simulations. The focus of the assessment is control-to-output transfer functions. In the triple phase shift modulation, there are three relevant control-to-output transfer functions, representing the effect of perturbations in each of the three control inputs on the output voltage. Similarly, there are two relevant control-to-output transfer functions for the dual phase shift modulation, and one for the single phase shift modulation. Magnitude plots of the frequency responses for each modulation strategy are shown in Fig. 10. Parameters used in the switching simulation are shown in Table III. Simulations include nonideal behaviors such as deadtime, control delays, and converter lossess. The control inputs for each modulation strategy were chosen such that the steady-state output voltage would be approximately 28 V in all three cases. For the triple phase shift case, the inputs were $d_\phi = 0.25$, $d_p = 0.435$, and $d_s = 0.85$. For the dual phase shift case, the inputs were $d_\phi = 0.25$, $d_p = d_s = 0.775$. For the single phase shift case, the inputs were $d_\phi = 0.2$, $d_p = d_s = 1$.

The final validation experiment considers the closed-loop transient response during a step change in voltage reference. The results are measured by logging data from the DSP during the experiment. This allows the sampled voltage and internal control variables to be observed experimentally. Data are logged from the DSP at a rate of 8 kHz. Load and hardware parameters are the same as those used in the previous tests, but the input voltage is fixed at 17 V. Results are shown in Fig. 11. The top plot shows sampled voltage and the bottom shows the phase shift calculated by the controller. Because a closed-loop system is used, the phase shift is not specified as an exogenous input. Instead, it is calculated internally as the output of the voltage controller. The action of the controller ensures that in a steady state, the output voltage is equal to the voltage reference. In terms of the model equations, the steady-state condition $v_{o0} = v_{\text{ref}}$ allows even the original model to predict output voltage with zero steady-state error. This is shown in the top plot of Fig. 11. However, in order to satisfy this relationship, all of the errors due to the first harmonic approximation are confined to

the phase shift. In contrast, the proposed modeling framework is able to predict both phase shift and output voltage accurately. This is a significant advantage in analyzing converter behavior. For instance, ZVS conditions for DAB converters are typically specified in terms of phase shift and voltage conversion ratio. The improved model is therefore capable of identifying ZVS operation, whereas the large-signal error of the original model precludes this type of analysis.

VII. Conclusion

The modeling framework proposed in this study extends the functionality of the existing GAM-based DAB models without significantly increasing the complexity. The new framework improves on the original model by including more general modulation strategies and by eliminating steady-state errors caused by the truncation of the Fourier series. This produces fully continuous-time models that are accurate over a wide range of converter operating conditions. The framework is proposed as a general tool: it is applicable to both open- and closed-loop operation and supports both large- and small-signal model development.

While the methods proposed here are useful for modeling a single converter, one of the motivations driving this line of research is the development of computationally efficient models for multiconverter systems. The large-signal accuracy of the proposed framework opens the door for system-level applications, and methods for semiexplicit DAE models are already well established in the traditional power system analysis. Future work in this study will continue to explore the challenges of system-level model construction, with the objective of identifying methods and models that are accessible to both power electronics and power systems research communities.

Appendix

We consider the linearization of $f(x, y, u)$ and $g(x, y, u)$. Large-signal states/inputs (x, y, u) can be broken into steady-state operating points (denoted by capital letters) and small-signal deviations.

$$x = X + \tilde{x}, \quad y = Y + \tilde{y}, \quad u = U + \tilde{u}. \tag{101}$$

The first-order Taylor series expansion of $f(\cdot)$ is

$$\dot{x} = \dot{X} + \dot{\tilde{x}} \approx f(X, Y, U) + \frac{\partial f}{\partial x}\tilde{x} + \frac{\partial f}{\partial y}\tilde{y} + \frac{\partial f}{\partial u}\tilde{u} \tag{102}$$

where $\frac{\partial f}{\partial x}$, $\frac{\partial f}{\partial y}$, and $\frac{\partial f}{\partial u}$ are evaluated at (X, Y, U). By definition, $\dot{X} = f(X, Y, U) = 0$, so

$$\dot{\tilde{x}} = \frac{\partial f}{\partial x}\tilde{x} + \frac{\partial f}{\partial y}\tilde{y} + \frac{\partial f}{\partial u}\tilde{u}. \tag{103}$$

Similarly, the Taylor series expansions of $g(\cdot)$ is

$$0 = g(X, Y, U) + \frac{\partial g}{\partial x}\tilde{x} + \frac{\partial g}{\partial y}\tilde{y} + \frac{\partial g}{\partial u}\tilde{u}. \tag{104}$$

Again, derivatives are evaluated at (X, Y, U), and $0 = g(X, Y, U)$. An expression for $\tilde{y}$ may be found by rearranging the following:

$$\tilde{y} = \left(\frac{\partial g}{\partial y}\right)^{-1}\left(-\frac{\partial g}{\partial x}\tilde{x} - \frac{\partial g}{\partial u}\tilde{u}\right). \tag{105}$$

Substituting this expression into (103) eliminates $\tilde{y}$. The resulting equation is

$$\dot{\tilde{x}} = \frac{\partial f}{\partial x}\tilde{x} - \frac{\partial f}{\partial y}\left(\frac{\partial g}{\partial y}\right)^{-1}\left(\frac{\partial g}{\partial x}\tilde{x} + \frac{\partial g}{\partial u}\tilde{u}\right) + \frac{\partial f}{\partial u}\tilde{u} \tag{106}$$

$$= A\tilde{x} + B\tilde{u} \tag{107}$$

where A and B correspond to the expressions in (79) and (80), respectively.

References

[1] R. W. A. A. DeDoncker, D. M. Divan, and M. H. Kheraluwala, "A three-phase soft-switched high-power-density dc/dc converter for high-power applications," *IEEE Trans. Ind. Appl.*, vol. 27, no. 1, pp. 63–73, Jan./Feb. 1991.

[2] M. N. Kheraluwala, R. W. Gascoigne, D. M. Divan, and E. D. Baumann, "Performance characterization of a high-power dual active bridge dc-to-dc converter," *IEEE Trans. Ind. Appl.*, vol. 28, no. 6, pp. 1294–1301, Nov./Dec. 1992.

[3] G. C. Verghese, M. E. Elbuluk, and J. G. Kassakian, "A general approach to sampled-data modeling for power electronic circuits," *IEEE Trans. Power Electron.*, vol. PE-1, no. 2, pp. 76–89, Apr. 1986.

[4] C. Zhao, S. D. Round, and J. W. Kolar, "Full-order averaging modelling of zero-voltage-switching phase-shift bidirectional dc–dc converters," *IET Power Electron.*, vol. 3, no. 3, pp. 400–410, 2010.

[5] F. Krismer and J. W. Kolar, "Accurate small-signal model for the digital control of an automotive bidirectional dual active bridge," *IEEE Trans. Power Electron.*, vol. 24, no. 12, pp. 2756–2768, Dec. 2009.

[6] L. Shi, W. Lei, Z. Li, J. Huang, Y. Cui, and Y. Wang, "Bilinear discrete-time modeling and stability analysis of the digitally controlled dual active bridge converter," *IEEE Trans. Power Electron.*, vol. 32, no. 11, pp. 8787–8799, Nov. 2017.

[7] A. Rodríguez, A. Vãzquez, D. G. Lamar, M. M. Hernando, and J. Sebastin, "Different purpose design strategies and techniques to improve the performance of a dual active bridge with phase-shift control," *IEEE Trans. Power Electron.*, vol. 30, no. 2, pp. 790–804, Feb. 2015.

[8] H. Qin and J. W. Kimball, "Solid-state transformer architecture using ac–ac dual-active-bridge converter," *IEEE Trans. Ind. Electron.*, vol. 60, no. 9, pp. 3720–3730, Sep. 2013.

[9] B. Hua, M. Chunting, W. Chongwu, and S. Gargies, "The dynamic model and hybrid phase-shift control of a dual-active-bridge converter," in *Proc. 34th Annu. Conf. IEEE Ind. Electron.*, 2008, pp. 2840–2845.

[10] R. D. Middlebrook and S. Cuk, "A general unified approach to modelling switching-converter power stages," in *Proc. IEEE Power Electron. Spec. Conf.*, 1976, pp. 18–34.

[11] K. Zhang, Z. Shan, and J. Jatskevich, "Large- and small-signal average-value modeling of dual-active-bridge dc-dc converter considering power losses," *IEEE Trans. Power Electron.*, vol. 32, no. 3, pp. 1964–1974, Mar. 2017.

[12] F. Zhang, M. M. U. Rehman, R. Zane, and D. Maksimović, "Improved steady-state model of the dual-active-bridge converter," in *Proc. IEEE Energy Convers. Congr. Expo.*, 2015, pp. 630–636.

[13] H. Qin and J. W. Kimball, "Generalized average modeling of dual active bridge dc-dc converter," *IEEE Trans. Power Electron.*, vol. 27, no. 4, pp. 2078–2084, Apr. 2012.

[14] S. R. Sanders, J. M. Noworolski, X. Z. Liu, and G. C. Verghese, "Generalized averaging method for power conversion circuits," *IEEE Trans. Power Electron.*, vol. 6, no. 2, pp. 251–259, Apr. 1991.

[15] S. Cooper, A. Klem, M. H. Nehrir, and H. Ga, "An improved state-space averaged model of a dual active bridge converter for use in acausal system modeling," in *Proc. North Am. Power Symp.*, 2016, pp. 1–5.

[16] S. S. Shah and S. Bhattacharya, "Large & small signal modeling of dual active bridge converter using improved first harmonic approximation," in *Proc. IEEE Appl. Power Electron. Conf. Expo.*, 2017, pp. 1175–1182.

[17] J. A. Mueller and J. W. Kimball, "Model-based determination of closed-loop input impedance for dual active bridge converters," in *Proc. IEEE Appl. Power Electron. Conf. Expo.*, Mar. 2017, pp. 1039–1046.

[18] J. Huang, Y. Wang, Z. Li, and W. Lei, "Unified triple-phase-shift control to minimize current stress and achieve full soft-switching of isolated bidirectional dc-dc converter," *IEEE Trans. Ind. Electron.*, vol. 63, no. 7, pp. 4169–4179, Jul. 2016.

[19] B. Zhao, Q. Song, and W. Liu, "Power characterization of isolated bidirectional dual-active-bridge dc-dc converter with dual-phase-shift control," *IEEE Trans. Power Electron.*, vol. 27, no. 9, pp. 4172–4176, Sep. 2012.

[20] B. Zhao, Q. Yu, and W. Sun, "Extended-phase-shift control of isolated bidirectional dc-dc converter for power distribution in microgrid," *IEEE Trans. Power Electron.*, vol. 27, no. 11, pp. 4667–4680, Nov. 2012.

[21] M. L. Crow, "Numerical integration," in *Computational Methods for Electric Power Systems*, 3rd ed. Boca Raton, FL, USA: CRC Press, 2016.

[22] P. T. Krein, J. Bentsman, R. M. Bass, and B. L. Lesieutre, "On the use of averaging for the analysis of power electronic systems," *IEEE Trans. Power Electron.*, vol. 5, no. 2, pp. 182–190, Apr. 1990.

[23] D. Gonzalez-Agudelo, A. Escobar-Mejía, and H. Ramirez-Murrillo, "Dynamic model of a dual active bridge suitable for solid state transformers," in *Proc. 13th Int. Conf. Power Electron.*, 2016, pp. 350–355.

[24] B. Zhao, Q. Song, W. Liu, and Y. Sun, "Dead-time effect of the high-frequency isolated bidirectional full-bridge dc–dc converter: Comprehensive theoretical analysis and experimental verification," *IEEE Trans. Power Electron.*, vol. 29, no. 4, pp. 1667–1680, Apr. 2014.

[25] D. Segaran, D. G. Holmes, and B. P. McGrath, "Enhanced load step response for a bidirectional dc–dc converter," *IEEE Trans. Power Electron.*, vol. 28, no. 1, pp. 371–379, Jan. 2013.

Jacob A. Mueller (S'12) received the B.S. and M.S. degrees in electrical and computer engineering from Missouri University of Science and Technology, Rolla, MO, USA, in 2012 and 2014, respectively, where he is currently working toward the Ph.D. degree in electrical engineering.

His research interests include modeling and control of power electronic converters, microgrid stability, and nonintrusive load monitoring.

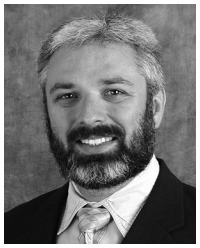

Jonathan W. Kimball (M'96–SM'05) received the B.S. degree in electrical and computer engineering from Carnegie Mellon University, Pittsburgh, PA, USA, in 1994, the M.S. degree in electrical engineering and the Ph.D. degree in electrical and computer engineering from the University of Illinois at Urbana-Champaign (Illinois), Champaign, IL, USA, in 1996 and 2007, respectively.

From 1996 to 1998, he worked for Motorola, Phoenix, AZ, USA, designing IGBT modules for industrial applications. He then joined Baldor Electric, Fort Smith, AR, USA, where he designed industrial adjustable speed drives ranging 1–150 hp. In 2003, he returned to Illinois as a Research Engineer (later a Senior Research Engineer). Later in 2003, he co-founded SmartSpark Energy Systems, Inc., in Champaign, IL, USA, and served as the Vice President of Engineering. He joined Missouri S&T (formerly the University of Missouri-Rolla) in 2008 as an Assistant Professor, and was promoted to Associate Professor (with tenure) in 2014. He was named a Deans Scholar in 2016.

Dr. Kimball is a member of Eta Kappa Nu, Tau Beta Pi, and Phi Kappa Phi. He is a licensed Professional Engineer in the State of Illinois. He served as the General Chair of the IEEE Applied Power Electronics Conference in 2017.